Electromagnetic instability of thin reconnection layers: Comparison of three-dimensional simulations with MRX observations

V. Roytershteyn,[1] S. Dorfman,[2,a)] W. Daughton,[3] H. Ji,[2] M. Yamada,[2] and H. Karimabadi[1,b)]
[1]*SciberQuest, Inc., Del Mar, California 92014, USA*
[2]*Princeton Plasma Physics Laboratory, Princeton, New Jersey 08543, USA*
[3]*Los Alamos National Laboratory, Los Alamos, New Mexico 87545, USA*

(Received 1 October 2012; accepted 4 January 2013; published online 21 June 2013)

The influence of current-aligned instabilities on magnetic reconnection in weakly collisional regimes is investigated using experimental observations from Magnetic Reconnection Experiment (MRX) [M. Yamada *et al.*, Phys. Plasmas **4**, 1936 (1997)] and large-scale fully kinetic simulations. In the simulations as well as in the experiment, the dominant instability is localized near the center of the reconnection layer, produces large perturbations of the magnetic field, and is characterized by the wavenumber that is a geometric mean between electron and ion gyroradii $k \sim (\rho_e \rho_i)^{-1/2}$. However, both the simulations and the experimental observations suggest the instability is not the dominant reconnection mechanism under parameters typical of MRX. © *2013 AIP Publishing LLC*. [http://dx.doi.org/10.1063/1.4811371]

I. INTRODUCTION

Magnetic reconnection remains one the most challenging and fascinating problems in plasma physics. Small-scale turbulence is frequently invoked in theoretical models of reconnection as a microscopic mechanism responsible for breaking the frozen-in condition. Among all of the possible types of turbulence, the fluctuations driven by current-aligned instabilities are of particular interest since they are thought to be naturally associated with reconnection current sheets. One of the frequently discussed causes of microscopic turbulence near the reconnection sites is the Lower-Hybrid Drift Instability (LHDI).[1–3] Indeed, electromagnetic fluctuations in the lower-hybrid frequency range are frequently observed in the vicinity of reconnection sites in both space (e.g., Refs. 4–9) and laboratory plasmas (e.g., Refs. 10–12). However, it remains unclear if the observed fluctuations play a key role in the reconnection process itself or are instead relatively passive accompaniments.

In this paper, we use large-scale three-dimensional (3D) kinetic simulations and experimental observations from Magnetic Reconnection Experiment (MRX)[13] to investigate the role of magnetic fluctuations experimentally observed near the X-line. MRX is a well-diagnosed compact laboratory experiment dedicated to studies of magnetic reconnection. It provides an excellent testbed to verify and challenge theoretical models. The motivation for the present analysis is two-fold. First, identification of the mechanism responsible for decoupling the electron fluid from the magnetic field in weakly collisional regimes achievable in MRX has proven challenging. Careful analysis of the structure of experimentally observed electron-scale reconnection layers revealed significant disagreement with the predictions of two-dimensional (2D) kinetic simulations.[14–17] Specifically, the appropriately normalized thickness of these layers in MRX is 3–5 times higher than the simulation results. Since the thickness of the reconnection layer is determined by the mechanism that decouples electrons from the magnetic field (hereafter, we will refer to this as the reconnection mechanism), this discrepancy suggests that this mechanism in MRX is of different origin compared to the 2D simulations. At the same time, recent highly resolved spacecraft observations demonstrated excellent agreement with 2D simulations, indicating that at least under some conditions reconnection layers with thickness of the order of electron inertial length are observable in nature.[18] Therefore, it is natural to assume that the magnetic fluctuations observed in MRX produce large contributions to the reconnection mechanism and are primarily responsible for the observed discrepancy.

More generally, the very existence of magnetic fluctuations observed in MRX near the X-line is of great theoretical interest. It has long been realized that in the anti-parallel reconnection configuration under conditions typical of MRX, most of the well-known current-driven instabilities are stable near the center of the current sheet. This is related to large local values of plasma beta, which is stabilizing for LHDI, and to the typical relation between ion and electron temperatures $T_i > T_e$, which tends to stabilize streaming instabilities. Since the same conditions are frequently encountered in many other systems of interest, such as the Earth's magnetopause, the problem is rather generic. In this regard, the electromagnetic instability of lower-hybrid origin capable of penetrating the vicinity of the X-line attracted particular attention (Ref. 19 and references therein). This mode produces large perturbations of the magnetic field and is characterized by the wavenumber that is a geometric mean between electron and ion gyroradii $k \sim (\rho_e \rho_i)^{-1/2}$. Early analysis based on the linear theory and kinetic simulations of

a)Present address: Department of Physics and Astronomy, University of California, Los Angeles, California 90095, USA.
b)Also at the ECE Department, University of California, San Diego, California 92093, USA.

model equilibria suggested that the instability may be an effective reconnection mechanism (e.g., Refs. 20–22). However, we have recently demonstrated that this instability does not necessarily play an important role in actively reconnecting current sheets.[23] While it is observed in many kinetic simulations of reconnection (e.g., Refs. 22–24), the conditions under which the instability reaches large amplitude and influences the reconnection mechanism in collisionless kinetic simulations are rather restrictive: large asymmetry, low β, and small ratios of ion-to-electron temperatures $T_i < T_e$. While there is some support for these theoretical predictions from spacecraft observations,[5,7,25] a more careful verification from laboratory experiments is highly desirable.

Given the above discussion, the goals of this paper are (i) to identify the origin of the magnetic fluctuations observed in MRX and (ii) to understand their influence on the reconnection process. The organization of the paper is as follows: in Sec. II, we describe the parameters, geometry, and the initial conditions of the simulations used in this analysis. Section III contains a brief description of the experimental conditions in MRX and presents some details of how the fluctuations are measured. Section IV contains the main results. The conclusions of the paper, summarized in Sec. V, are as follows: (i) the observed fluctuations originate from the electromagnetic instability discussed above and (ii) they are not the dominant reconnection mechanism in weakly collisional regimes and are not responsible for the observed deviation of the electron layer structure from 2D simulation results.

II. FULLY KINETIC 3D SIMULATIONS

Throughout this paper, we compare results of two large-scale fully kinetic simulations with experimental observations. The first simulation is a driven collisionless simulation performed in an open-boundary geometry. It is a high mass ratio ($m_i/m_e = 900$) version of the simulations described in Ref. 23. This case is of relevance to the most collisionless discharges in MRX and is of great interest since the employed mass ratio is only a factor of two smaller than that of hydrogen $m_H/m_e \approx 1836$. The second simulation includes Coulomb collisions and employs initial conditions and aspects of geometry mimicking MRX. Since we are interested in modeling MRX experiments with no externally applied guide field (see Sec. III), neither of the simulations includes a guide field. Both simulations utilize high-performance particle-in-cell (PIC) code VPIC.[26,27]

The collisionless simulation employs asymmetric initial conditions. As we discuss below, some degree of asymmetry is always present in MRX. However, no attempt is made to match asymmetry in this simulation to any specific MRX discharge. The simulation is initialized with magnetic field of the form $\boldsymbol{B} = 0.5[(B_0 + B_1) - (B_0 - B_1)\tanh(x/\delta_0)]\boldsymbol{e}_z$. Here, indices "0" and "1" denote, respectively, asymptotic values on the high-β and low-β sides of the current sheet at $t = 0$. The local time-evolving quantities do not have an index. The initial particle distributions consist of two components, a Harris-like distribution $f_s = n_{cc}\cosh^{-2}(x/\delta_0)\exp[-m_s(\boldsymbol{v} - U_s\boldsymbol{e}_y)^2/(2T_s^0)]$, and an asymmetric Maxwellian component with density $n(x) = 0.5[(n_0 + n_1) - (n_0 - n_1)\tanh(x/\delta_0)]$ and temperature T_s^0. Here, δ_0 is the half-thickness of the initial current sheet chosen to be $\delta_0 = 0.5d_i^0$, where $d_s^0 = c/\omega_{ps}$, $\omega_{ps} = (4\pi n_0 q_s^2/m_s)^{1/2}$, m_s and q_s are, respectively, mass and charge of species s. The force balance across the layer dictates that $8\pi n_0(T_e^0 + T_i^0) + B_0^2 = 8\pi n_1(T_e^0 + T_i^0) + B_1^2 = 8\pi[n_{cc} + 0.5(n_1 + n_0)](T_e^0 + T_i^0)$. Note that the coordinate system used throughout this paper is different compared to Ref. 23 and matches the coordinate system traditionally used by MRX. The initial configuration is parameterized by the value of plasma $\beta_0 = 8\pi n_0(T_e^0 + T_i^0)/B_0^2$ and the ratio n_1/n_0 between densities on the low-β and the high-β sides. For the simulation described in this paper, $\beta_0 = 0.5$, $n_1/n_0 = 0.1$, and $T_i^0 = T_e^0$. The initial configuration does not correspond to an exact Vlasov equilibrium, but is in force balance and allows reconnection to develop after a few Alfvén times. The inflow boundaries are driven by applying electric field $E_y = -E_y^0\exp(-t/\tau)$, where $E_y^0 = 0.08B_0V_A^0/c$, $\tau = 20(\omega_{ci}^0)^{-1}$, $V_A^0 = d_i^0\omega_{ci}^0$, and $\omega_{cs}^0 = q_sB_0/(m_sc)$. In order to study the evolution of the system over a long time scale, the simulations employed open downstream boundary conditions that allow plasma and electromagnetic flux to leave the simulation domain.[28] Other numerical parameters are $\omega_{pe}^0/\omega_{ce}^0 = 1.75$, spatial domain $L_x \times L_y \times L_z = (10 \times 3 \times 10)\,d_i^0$ with $1024 \times 320 \times 1024$ cells, and time step $\Delta t\omega_{ce}^0 \approx 0.095$. The plasma at $t = 0$ was represented by 2×10^{11} computational particles. The overall dynamics of this simulation and the instabilities that develop closely resemble results from lower mass ratio simulations $m_i/m_e = 400$ described in Ref. 23. Fig. 1 presents an overview of this simulation at a fully developed stage $t\omega_{ci}^0 = 41$. A detailed analysis of the fluctuations and comparison with MRX observations is presented in Sec. IV.

In order to better reproduce the experimental conditions, we also conducted a series of simulations that include Coulomb collisions and aspects of MRX geometry. The simulation model extends the one previously used by us to conduct 2D simulations.[16,17] Coulomb collisions are treated with a Monte-Carlo approach[29] that has been extensively tested (e.g., Refs. 30 and 31) and previously used in reconnection simulations.[17,31,32] The simulations described here

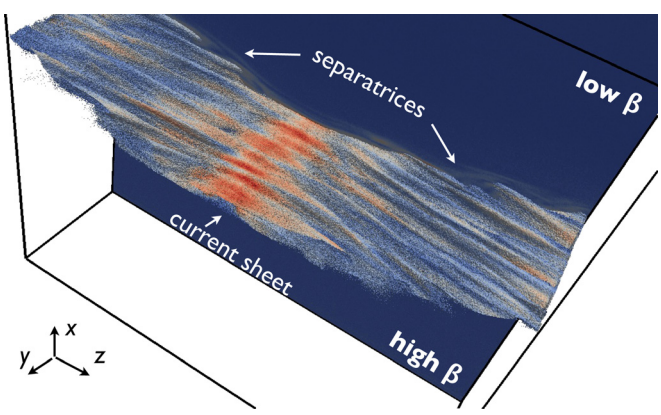

FIG. 1. Collisionless simulation with $m_i/m_e = 900$. Shown is an isosurface of constant density on the low-β side of the current sheet, colored by the magnitude of current density $|J|$. Instabilities of the central current sheet and very strong LHDI activity along low-β separatrices are clearly visible. Simulation parameters are specified in the text.

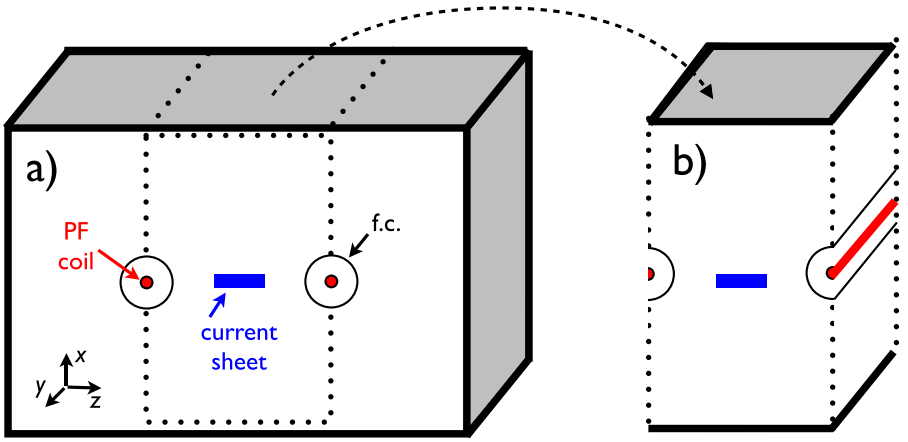

FIG. 2. Geometry of the MRX simulations: (a) 3D extension of the geometry used to conduct previous 2D simulations;[16,17] (b) reduced geometry utilized in this study. The shaded surfaces represent conducting boundary conditions for fields and reflecting boundary conditions for the particles. Periodic boundary conditions are imposed on unshaded surfaces. The reconnection is driven by ramping down y-current in prescribed regions of the simulation domain that mimic PF coils in MRX. The poloidal field coils are enclosed by flux cores (F.C.), which are modeled through absorbing particle boundary conditions.

are conducted in a slab geometry appropriate to the short-wavelength modes of interest, illustrated in the right panel of Fig. 2. The geometry and the initial conditions seek to mimic the pull phase of reconnection in MRX.[16] Specifically, the reconnection is driven by ramping down in time the prescribed current $I(t)$ in two regions of the simulation domain corresponding to MRX poloidal field (PF) coils (see Fig. 2). The functional form $I(t) = I_0[1 + 5\cos^2(\pi(t + t_0)/2\tau)]/6$ is chosen to model the time dependence of current in MRX PF coils. For the simulation considered $\tau = 150\omega_{ci}^0$ and $t_0 = 0.3\tau$. The initial magnetic field $\boldsymbol{B}(x, z)$ at $t = 0$ is due to the prescribed current I_0, while the particle distribution functions are of the form $f_s = n(x, z)\exp(-m_s v^2/2T_s^0)$, where $n(x, z)$ at $t = 0$ is chosen in such a way that the density profile during active reconnection phase $t \sim \tau/2$ resembles experimentally observed profiles. In this simulation, the initial temperatures of ions and electrons are equal $T_i^0/T_e^0 = 1$. Density and magnetic field profiles in MRX are characterized by a degree of radial asymmetry that is induced by toroidal effects. In order to mimic this asymmetry in the simulation, the current-carrying regions corresponding to the MRX PF coils are offset in the radial direction by 1/6 of simulation domain length. After the simulation is initialized at $t = 0$, it evolves self-consistently in response to the changing current $I(t)$. In order to reduce the cost of highly expensive 3D simulations, we utilized a reduced version of the geometry used in 2D[16,17] with periodic boundary conditions in y and z directions. The size of the simulation domain is $L_x \times L_y \times L_z \approx (8.8 \times 2.9 \times 11.5)d_i^0$ with $1202 \times 390 \times 1536$ cells. The simulation employs $m_i/m_e = 300$. The reference values of other parameters are $\omega_{pe}^0/\omega_{ce}^0 = 1$ and $\beta_e^0 = 8\pi n_o T_e^0/B_0^2 = 0.01$. However, these values correspond to a reference value of magnetic field B_0 created by the PF coils at $t = -t_0$ at a referenced position in the middle of the simulation domain.[16] More relevant are parameters corresponding to a developed reconnection phase $t \sim \tau/2$. For example, $\omega_{pe}/\omega_{ce} \approx 5$ at $t = \tau/2$ if the density is measured at the center of the current layer and the magnetic field on its shoulder. The local value of electron beta on the low-density side of the simulation domain at $t = \tau/2$ is $\beta_e \approx 0.35$. A snapshot of the MRX simulation is presented in Fig. 3, which illustrates the development of current sheet instabilities in this simulation.

At present, it is not feasible to conduct 3D explicit fully kinetic simulations of large-scale systems with realistic values of m_i/m_e and ω_{pe}/ω_{ce}. For any attempt to model experimental observations, an important choice is how to scale with m_i/m_e and ω_{pe}/ω_{ce} various quantities such as the system size or the relevant time scale. In this work, we utilize the same approach that was used and motivated in Refs. 16 and 17. The dimensions of the simulation domain are chosen to be comparable to the size of the experiment in terms of the ion inertial length d_i^0, while the time scales are normalized by ω_{ci}^0. The plasma β in the inflow region is chosen to be comparable to the experimental observations. The employed collisional model allows for a considerable flexibility in scaling of the collision frequency. Our approach is motivated by the results of 2D studies on how the structure of the electron reconnection layer depends on the regime of collisionality.[17] Specifically, we enforce the ratios between various frequencies to follow the same parametric dependence as the physical collision frequency (i.e., $\nu_{ee}/\nu_{ii} \propto (m_i/m_e)^{1/2}(T_i/T_e)^{3/2}$). The overall scaling factor is chosen to match the typical values of the ratio between the reconnection electric field and the Dreicer runaway critical electric field to the experiments of interest

$$E_D \equiv \sqrt{T_e m_e}\nu_{ee}/e. \quad (1)$$

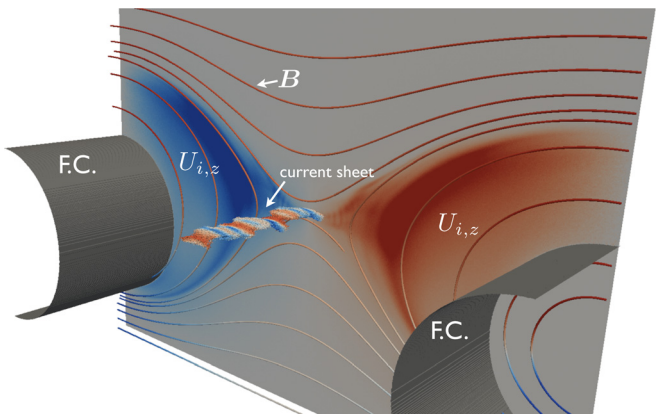

FIG. 3. Weakly collisional simulation performed in MRX geometry with $m_i/m_e = 300$. Shown is an isosurface of current density colored by the x-component of the electron flow velocity $U_{e,x}$ in order to highlight multiple instabilities of the central current sheet. The back panel shows ion outflow velocity $U_{i,z}$. Sample magnetic field lines and the flux core surfaces are also shown. Simulation parameters are specified in the text.

Assuming that the reconnection rate $cE/(BV_A)$ is comparable between the simulations and the experiments,[16] this implies that the collision frequency needs to be scaled as

$$\left(\frac{\nu_{ee}}{\omega_{ce}}\right)_{\text{sim}} = \left(\frac{\nu_{ee}}{\omega_{ce}}\right)_{\text{exp}} \left(\beta_e^* \frac{m_i}{m_e}\right)_{\text{sim}}^{-1/2} \left(\beta_e^* \frac{m_i}{m_e}\right)_{\text{exp}}^{1/2}, \quad (2)$$

where label "exp" and "sim" refer to the values in experiment and simulations, respectively. Here, β^* refers to β defined with pressure near the X-line and the edge magnetic field. Typical experimental values are $\beta_e^* \approx (0.3 - 0.5)$. Assuming that values of $\beta_e^* \sim T_e/(T_i + T_e)$ are close between simulations and experiment, relation (2) implies that ratio of the lower-hybrid frequency $\omega_{\text{LH}} = (\omega_{ce}\omega_{ci})^{1/2}$ to the electron collision frequency is also matched between the simulations and the experiment. This is important to achieve since the characteristic frequency and growth rate of the relevant instabilities are expected to scale as $\omega, \gamma \propto \omega_{\text{LH}}$. The typical values of β_e^* for our 3D simulations are $\beta_e^* \approx (0.25 - 0.7)$.

In order to measure properties of electromagnetic fluctuations in the simulations, we have constructed a dedicated diagnostic. At a number of locations in the simulation domain, the local values of electric and magnetic fields $E_{x,y,z}(t)$ and $B_{x,y,z}(t)$ are saved with a high time resolution $\delta t \omega_{\text{LH}}^0 = 0.25\pi$. In the simulations described in this paper, the spatial locations of such "virtual probes" are organized in a grid pattern in the (x, z) plane with a typical spacing δx and δz of a few d_e^0. The y-spacing δy is equal to one cell. The information obtained by this diagnostic can be post-processed to compute various properties of the fluctuating fields, such as spectra, cross-correlations, etc. All of the spectra presented in this paper were obtained during a stage with fully developed reconnection over a time interval where fluctuation amplitude remains approximately constant.

III. MRX OBSERVATIONS

The MRX is a compact toroidal device dedicated to studies of magnetic reconnection.[13] It consists of a cylindrical vacuum vessel with the inner radius $R_0 = 76.2$ cm. Two current-carrying toroidal coils (flux cores) of radius 37.5 cm inside the vessel both produce the plasma and drive the reconnection. The surface-to-surface separation between the flux cores is $Z_0 = 40$ cm. In the so-called pull scenario investigated here, the current in the flux cores is ramped down after the plasma formation period, initiating reconnection in a narrow toroidal current sheet between the flux cores. The present experiments to investigate electromagnetic fluctuations were performed in hydrogen or deuterium plasmas with the following typical parameters: electron density $n_e = (0.5 - 20) \times 10^{13}\text{cm}^{-3}$, electron temperature near the center of the current sheet $T_e = (5 - 15)$eV, magnetic field at the edge of the current sheet $B = (150 - 300)$G. The ion temperature was not directly measured in these experiments, but is estimated from the radial force balance across the current layer to be in the range $T_i = (5 - 15)$eV near the layer center. This range is consistent with previous ion temperature measurements performed in MRX helium discharges.[33] In more collisional discharges, the Coulomb collisions tend to enforce $T_e \sim T_i$, while in more collisionless discharges, ion temperature is generally higher than the corresponding electron temperature at the layer center.

The slab geometry of the simulations discussed in this paper corresponds to a narrow toroidal wedge of MRX. The employed coordinate system is as follows: z denotes the direction of the reconnecting magnetic field, R (or x) refers to the radial (inflow) direction, and y is the electron flow direction out-of-plane, corresponding to the toroidal direction in MRX (see Fig. 2).

In order to measure the details of the reconnection process, a number of electrostatic and magnetic diagnostic probes are placed in the reconnection layer. These include fine structure probe arrays, Langmuir probes, and magnetic fluctuation probes. A single fine structure probe consists of an array of up to 50 magnetic pickup coils in a 4.25 mm diameter glass tube. Each coil measures one component of the magnetic field at one radial location. The total radial coverage is close to 20 cm with a maximum resolution of 3.75 mm. When many of these probes are placed at different z locations, the evolution of the reconnection layer geometry may be tracked over a single discharge. All of the relevant measurements presented in the paper were performed with an array of 7 probes with 35 coils per probe. Langmuir probes are the primary electrostatic diagnostic used to determine plasma density and temperature. In the experiments described here, triple Langmuir probes with tip area of approximately 3 mm^2 were employed. Electron temperature is obtained from the potential difference between a floating tip and a positively biased tip. Plasma density is calculated using the ion saturation current drawn from the probe and the measured temperature.

Perhaps the most important diagnostic for the present set of experiments is a set of magnetic fluctuation probes that measure the high frequency components of B. These consist of up to four magnetic pickup coils connected to a small amplifier board placed in the probe shaft. The addition of this current buffer to the circuit ensures that magnetic signals at frequencies on the order of the lower hybrid frequency $\nu_{\text{LH}} = (10 - 15)$MHz are not dominated by noise pickup. In order to measure correlations between fluctuation signals and determine the phase velocity of the observed modes, two or more fluctuation probes must be placed in close proximity. This is achieved by placing one of the probes on a movable ball flange. By adjusting the position of the probe on the ball flange, the two probes may be brought to within a few millimeters of each other for detailed phase shift measurements.

The experimental measurements of the fluctuating magnetic field presented in this paper are typically assembled over multiple discharges. For example, the measurements of the radial profile of the fluctuations presented in Sec. IV were obtained from 215 reproducible discharges using the following procedure. In each discharge, the fluctuating component of B_z at $z = 0$ was measured by a four channel probe at four different radial locations separated by 2 cm. For each discharge, a 5 μs window is chosen centered at the time the reconnection electric field peaks. To produce a radial power

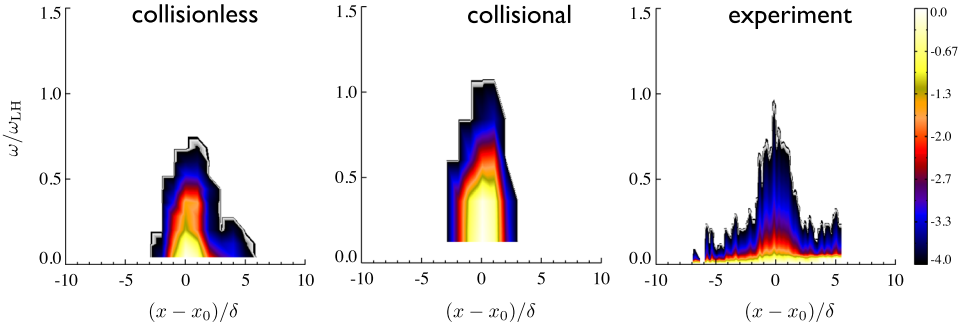

FIG. 4. Radial profile of the magnetic fluctuation frequency spectrum $\delta B^2(x,\omega)=\sum_{k_y}|B_z(\omega,x,k_y,z_0)|^2$ across the reconnection layer in the experiment (experiment), collisionless simulation (collisionless), and weakly collisional simulation in MRX geometry (collisional). Here, z_0 refers to the average z-coordinate of the X-line. In all cases, the X-line is located close to $x=x_0$ (within the resolution of the diagnostics). The quantity plotted in each panel is $\ln[\delta B^2(x,\omega)/B_0^2]$, where $B_0^2=\max[\delta B^2(x,\omega)]$ is the maximum of the respective spectrum.

spectrum, the $215\times 4=860$ individual spectra were binned based on the distance of each measurement from the current center position R_0 during the selected time period. The results are then compiled over the discharges.

IV. COMPARISON OF THE FLUCTUATIONS OBSERVED IN MRX WITH THE RESULTS OF FULLY KINETIC SIMULATIONS

As we discussed in the introduction, there is a considerable amount of theoretical and observational evidence indicating that current sheets undergoing reconnection tend to become unstable against a broad spectrum of electromagnetic instabilities. Such instabilities can in principle affect the reconnection mechanism in a number of ways, for example, by inducing anomalously large transport of electron momentum. However, most of the instabilities known to be effective at producing momentum transport cannot be excited near the center of the reconnection layer under conditions typical of MRX experiments discussed here (i.e., very small guide field and $T_i\gtrsim T_e$). As such, these instabilities cannot directly influence the reconnection process. In this regard, the fluctuations of magnetic field observed within reconnection layers in MRX and in kinetic simulations are of great interest (e.g., Refs. 11, 19, and 23 and references therein). Indeed, as is illustrated by Fig. 4, these relatively low-frequency magnetic fluctuations peak near the X-line. The characteristic width of the fluctuation amplitude profile is comparable to the thickness of the current layer δ. In contrast, the fluctuations of the electric field (not shown) in both the experiment and in the simulations tend to be localized slightly upstream of the reconnection layer (e.g., Refs. 10, 23, and 34) in the regions of small β. They originate from the well-known short-wavelength lower-hybrid drift instability with characteristic wavelength $k\rho_e\sim 1$.[1]

More detailed information about the spectra of the observed magnetic fluctuations is presented in Fig. 5, which shows $\omega-k_y$ spectra of B_z close to the X-line. The salient features of the presented spectra are as follows:

(1) The dominant fluctuations propagate along the direction of the electron drift, $\omega/k_y>0$.
(2) The dominant modes observed in the simulations are characterized by wavenumbers of the order of $k_0=(\rho_i\rho_e)^{-1/2}$ and frequencies in the range $\omega<\omega_{LH}$. The peak of the spectra corresponds to wavenumber $k\approx k_0$ and frequency $\omega\sim k_0 v_{th,i}$.
(3) The dominant modes in the experimentally measured spectrum correspond to the same direction of propagation and roughly the same wavenumber and frequency

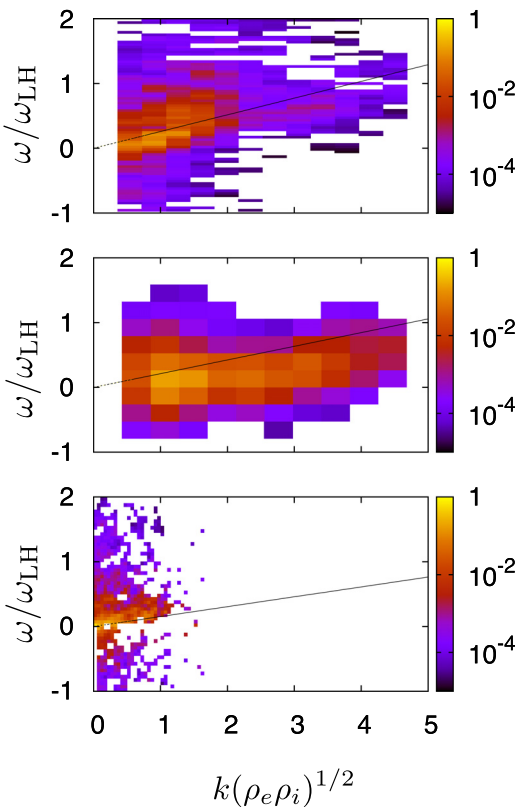

FIG. 5. Comparison of a typical $\omega-k_y$ spectrum $|\delta B(k_y,\omega)|^2$ observed in MRX deuterium discharges (bottom panel) with the spectra measured in the collisionless (top) and weakly collisional (middle) simulations. All spectra are normalized to their respective peak value δB^2_{max}. In each panel, the thin black line corresponds to $\omega=kv_{th,i}$. Note that with the normalizations utilized here, $v_{th,i}/[\omega_{LH}(\rho_e\rho_i)^{1/2}]=[(T_i/T_e)(m_e/m_i)]^{1/4}$. In order to compute the slope of the curve $\omega=kv_{th,i}$ for the experimental plot, $T_i/T_e=2$ was assumed. The normalizations for simulation data are computed as follows: $\rho_s=v_s/\omega_{cs}$, $v_s=[2P_{yy,s}/(n_s m_s)]^{1/2}$, stress tensor $P_{ij,s}$, and particle density n_e are measured at the center of the reconnection layer, while ω_{cs} is computed with the magnetic field measured at the edge of the reconnection layer. The value of v_s in the experiment is computed using temperature measured by a Langmuir probe.

range as in the simulation spectra. To illustrate this point, we estimate $k(\rho_e\rho_i)^{1/2}$ corresponding to other characteristics scale-lengths. For example, $k=\rho_e^{-1}$ corresponds to $k(\rho_e\rho_i)^{1/2}=(\rho_i/\rho_e)^{1/2}=(T_i/T_e)^{1/4}(m_i/m_e)^{1/4}$. This is approximately $7.8(T_i/T_e)^{1/4}$ for the deuterium discharges in MRX. Similarly, $k=d_e^{-1}$ corresponds to $k(\rho_e\rho_i)^{1/2}=\sqrt{\beta_e}(\rho_i/\rho_e)^{1/2}$. Taking representative $\beta_e=0.3-0.5$, this is equal to $(4.2-5.5)(T_i/T_e)^{1/4}$. The wave numbers corresponding to ion scales are $k=\rho_i^{-1}$, corresponding to $k(\rho_e\rho_i)^{1/2}=(\rho_e/\rho_i)^{1/2}$, which is $0.13(T_e/T_i)^{1/4}$ under the same assumptions; and $k=d_i^{-1}$, which translates to $k(\rho_e\rho_i)^{1/2}=\sqrt{\beta_i}(\rho_e/\rho_i)^{1/2}\approx(0.07-0.09)(T_e/T_i)^{1/4}$. We conclude that the experimentally observed wave number range observed in Fig. 5 is most consistent with $k(\rho_e\rho_i)^{1/2}\approx 1$ and is significantly separated from other possible characteristic scales.

(4) The characteristic phase velocity of the fluctuations in consistent between the simulations and the experiment.

Note that the frequency resolution in the weakly collisional simulation (middle panel) is limited since the radial profiles of magnetic field, density, and temperature are evolving on a time scale comparable to the duration of the interval used for this measurement. The experimental data are obtained using two three-component fluctuation probes at $R=40$ cm, $z=0$ cm separated by 6.6 mm in the toroidal direction (see Sec. III for details). The shown spectra are compiled across multiple similar discharges.

Based on the results summarized by Figures 4 and 5, we conclude that the properties of the magnetic fluctuations observed in MRX bear considerable resemblance to those observed in the simulations. The characteristic frequencies and the wavenumbers in all cases correspond to those expected for the instability identified in Ref. 19. Consequently, the characteristic phase velocity of the experimentally observed fluctuations match the simulations when it is normalized to a characteristic value $\omega_{\mathrm{LH}}(\rho_e\rho_i)^{1/2}$. Moreover, in both the experiment and in the simulations, the dominant modes are resonant with the ions, $\omega\approx v_{th,i}k$. Interestingly, the phase velocity of the fluctuations in the experiment is also consistent with the magnitude of the electron drift U_e. On the other hand, $|\omega/k_y|\ll|U_e|$ in the simulation data. Given the differences in the structure of reconnection layers observed between simulations and the experiment (see more discussion below), we conclude that the phase velocity of the fluctuations does not strongly depend on the magnitude of the electron drift.

Having established the correspondence between the fluctuations observed in the simulations and in the experiment, we now turn to the analysis of their influence on the reconnection process. The most direct assessment of the role of observed instabilities is offered by comparing 3D simulations with equivalent 2D cases. Indeed, the simulations discussed here possess a large-scale 2D symmetry imposed by the initial and boundary conditions. Therefore, various quantities measured in 3D simulations can be averaged over the symmetry direction (y) and directly compared against 2D runs. Since 2D geometry excludes perturbations with finite k_y, any difference between otherwise identical 2D and 3D cases has to be attributed to the influence of instabilities. This argument can be made quantitative by considering the average force balance near the X-line

$$m_e\langle n_e d\boldsymbol{V}_e/dt\rangle=-e\langle n_e\boldsymbol{E}\rangle-\langle\nabla\cdot\boldsymbol{P}_e\rangle-e\langle n_e(\boldsymbol{V}_e/c)\times\boldsymbol{B}\rangle+\langle\boldsymbol{R}_{ei}\rangle, \quad (3)$$

where $\langle A\rangle$ denotes average over y of quantity A. The friction force $\boldsymbol{R}_{ei}$ represents collisional momentum exchange between electrons and ions. Each nonlinear term in Eq. (3) can be split into contributions from average parts and contribution from the fluctuations. For example, $\langle AB\rangle=\langle\delta A\delta B\rangle+\langle A\rangle\langle B\rangle$, where δA refers to the fluctuating part of $A=\langle A\rangle+\delta A$. Similarly, $\langle ABC\rangle=\langle A\rangle\langle B\rangle\langle C\rangle+\langle A\rangle\langle\delta A\delta B\rangle+\langle B\rangle\langle\delta A\delta C\rangle+\langle C\rangle\langle\delta A\delta B\rangle+\langle\delta A\delta B\delta C\rangle$. Assuming their amplitude is sufficiently large, the fluctuations of the type discussed here can in principle produce sizable contributions to the average force balance through such terms as fluctuation-induced drag $\langle\delta n\delta E\rangle$, etc. (e.g., Refs. 21–23). Such modifications of the average force balance would be necessarily accompanied by changes in the structure of the reconnection layer. For example, the average thickness of the current layer was 3 times higher compared to the respective 2D cases in the most unstable simulations described in Ref. 23. However, the results of those collisionless simulation are not directly relevant to MRX since the values of some of the critical parameters do not correspond to typical MRX conditions (e.g., simulations assume very low values of plasma $\beta<0.1$ and $T_i^0<T_e^0$ in the inflow region, while typical MRX values are $\beta>0.5$, and $T_i>T_e$).

In contrast, fluctuations play comparatively smaller role in the simulations discussed in this paper. As an example, Fig. 6 compares the current density in the 3D weakly collisional MRX simulation with its 2D counterpart. We observe that the current layer is on average about 25% wider in this 3D simulation compared to 2D. The observed differences in the structure of the reconnection layer are relatively small and certainly are not enough to explain the differences between 2D simulations and the experiment. Moreover, in a typical simulation, the instabilities do not reach large amplitude unless the reconnection layer is first compressed to the scales of a few electron gyroradii, which is smaller than the minimum thickness observed in the experiment (see more discussion below). Consistent with this notion, the typical root-mean-square (rms) amplitude $\langle\delta B^2\rangle^{1/2}$ of the fluctuating magnetic field observed in the experiment is a few Gauss (as shown in Fig. 7 below), which should be compared to the values of magnetic files on the shoulder of the electron layer of $B_0=150-250$G. In the simulations discussed in this paper, the rms amplitude is of the same order or higher, $\langle\delta B^2\rangle^{1/2}/B_0\lesssim 10\%$.

To summarize, our simulations demonstrated that the magnetic fluctuations observed in MRX likely originate from the long-wavelength instability with characteristic wavelength $k(\rho_e\rho_i)^{1/2}$ that has been identified previously in linear theory and many collisionless kinetic simulations. In contrast to early expectations based on considerations of model equilibria such as Harris current sheet, the instability does not always play an important role in current sheets undergoing active reconnection. Rather, the saturation

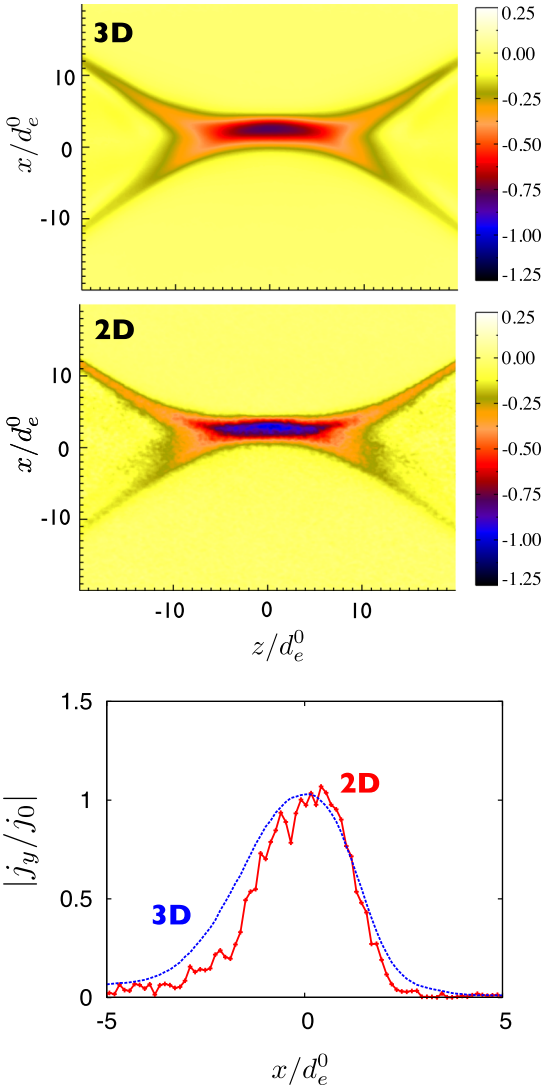

FIG. 6. Average current density $\langle j_y \rangle$ in the 3D weakly collisional case (top) and in its 2D equivalent (bottom). In the top two panels, j_y is normalized to its peak value in 2D case. The bottom panel shows x-profile of $|j_y|$ at $z = 0$.

amplitude is very sensitive to the details of equilibrium, such as the value of β, the degree of radial asymmetry between the two sides of the current sheet. The apparent discrepancy between the predictions drawn from analysis of static equilibria and the results of simulations focusing on the stage of developed reconnection is likely related to the constraints imposed on the growth rate of the relevant instabilities by the fast convection of the electron fluid through the reconnection region.[23] The simulations indicate that the fluctuations are unlikely to substantially modify the structure of the reconnection layer under conditions typical of MRX. However, only a small number of these highly expensive 3D fully kinetic simulations with finite collisionality have been performed, covering a rather limited range of parameters. In order to corroborate the simulation predictions concerning the possible influence of the instabilities on reconnection in MRX, we utilize the understanding gained from the simulations and linear theory to focus on two experimental results: the dependence of the fluctuation amplitude δB on the regime of collisionality and the dependence of the observed

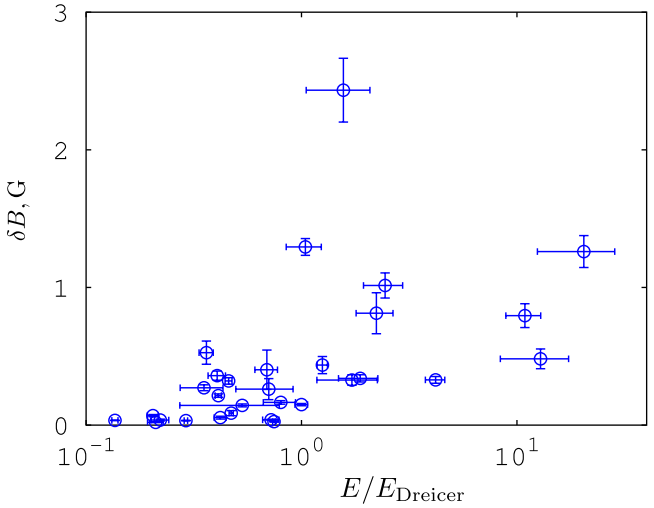

FIG. 7. Correlation of the fluctuation amplitude with the collisionality regime, as measured by ratio of reconnection electric field E to the critical Dreicer field E_D. Qualitatively similar dependence can be observed dynamically within a single discharge. The error bars are from an average over a 1.2 μs window around the time at which the current sheet passes by a fixed array of Langmuir probes at $R = 37.5$ cm.

width of the reconnection layer on the occurrence rate and the amplitude of the fluctuations.

We consider a set of 30 experimental discharges. The time selected for measurements in each shot correspond to the time at which the R location of the X-point passes by a fixed array of Langmuir probes located at $R = 37.5$ cm. At the crossing time, the plasma density at the X-point spans a wide range $(0.15 - 6) \times 10^{13}\mathrm{cm}^{-3}$, corresponding to a broad scan of collisionality regime $E_{\mathrm{Dreicer}} \propto n/T_e$. Electron temperature varies only by about a factor of two across these discharges. Fluctuation amplitudes were obtained by two three-component fluctuation probes in the outflow region. One probe is located at $z = -7.5$ cm, $R = 37.5$ cm; the second is at $z = 10.5$ cm, $R = 37.5$ cm. The data presented below are an average between the measurements of the two probes.

An important observation regarding the properties of magnetic fluctuations in MRX is that their amplitude increases with decreasing collisionality, as illustrated in Fig. 7 (see also Ref. 11). One attractive interpretation of this result is in terms of the increasing importance of fluctuation-induced momentum transport, as measured, for example, by $E/(\eta_S j)$, where E is the reconnection electric field and η_S is the Spitzer resistivity. On the other hand, one may regard the increase of the fluctuation amplitude as *a passive consequence* of the modifications in the structure of reconnection layers expected with decreasing collisionality. Indeed, as we demonstrated in Ref. 17 using 2D simulations, the contribution of the collisional electron-ion momentum exchange to the force balance near the X-line quickly diminishes as the ratio between reconnection electric field and the critical runaway field E_{Dreicer} defined by Eq. (1) approaches unity. As a consequence, the thickness of the reconnection layer δ/ρ_e in 2D simulations quickly decreases as E/E_{Dreicer} approaches one. As is demonstrated in Fig. 8, the experimental data certainly follow this trend, even if the absolute values of δ/ρ_e are significantly different between the experiment and the

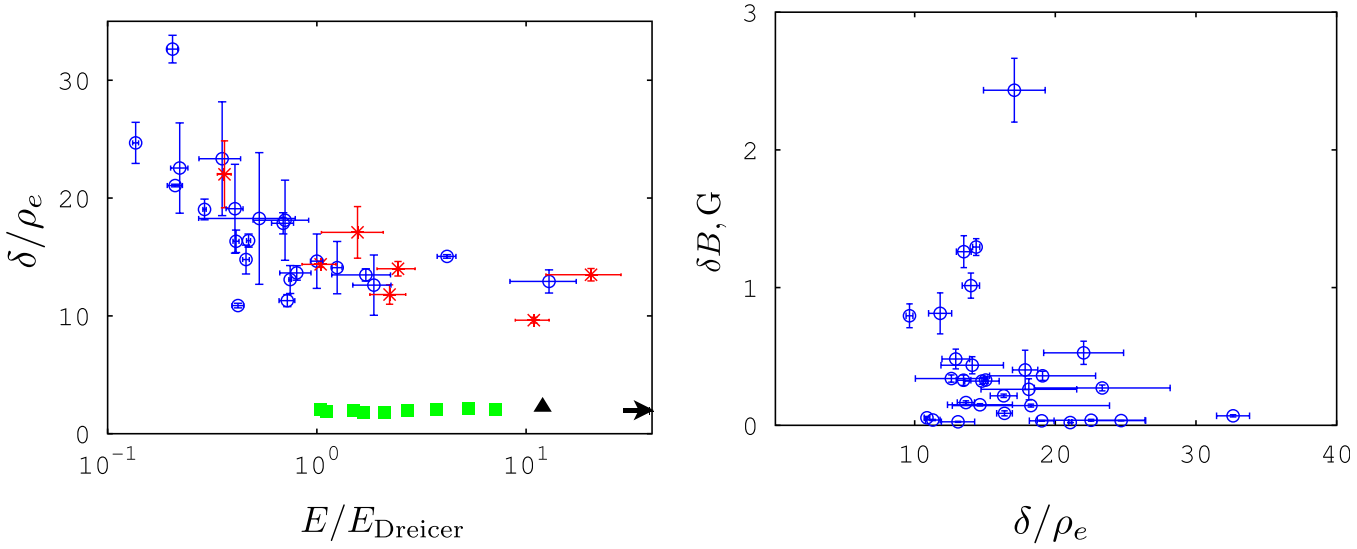

FIG. 8. Left: the width of the reconnection layer δ vs collisionality regime E/E_{Dreicer}. Experimental discharges are grouped into those with small fluctuation amplitude δB (○, $\delta B < 0.5$G) and those with significant fluctuations (*, $\delta B > 0.5$G). Simulations are represented by symbols ■ (2D cases with $E/E_{\mathrm{Dreicer}} > 1$), ▲ (3D weakly collisional), and → (3D collisionless with formally infinite E/E_{Dreicer}). Right: fluctuation amplitude δB vs the width of the reconnection layer. The error bars on the experimental data points are from an average over a 1.2 μs window around the time at which the current sheet passes by the probes. Layer thickness δ is defined as the half-width of the current profile at 40% of its maximum value as measured at the z location of the layer center. To compute electron gyro-radius ρ_e and E_{Dreicer}, the temperature and density were measured at the center of the electron layer, while B_z was measured at one δ upstream. The reconnection electric field E in the experimental data is the inductive field at the X-point obtained through magnetic flux integration.

2D simulations. Since the growth rate of the relevant instability increases with decreasing δ/ρ_e, it is quite natural that the amplitude of the fluctuations tend to be higher in cases with $E/E_{\mathrm{Dreicer}} \gtrsim 1$.

An understanding of the mechanism responsible for controlling the thickness of the experimentally observed reconnection layer is crucial for identification of the reconnection mechanism in MRX. Indeed, 2D simulations excluding the instabilities indicate that at $E/E_{\mathrm{Dreicer}} \gtrsim 1$, the collisional momentum exchange is largely ineffective and the reconnection electric field is supported predominantly by the divergence of the electron stress tensor. This necessarily requires that layer thickness collapses to the scales comparable to electron crossing orbit width (a few ρ_e).[17] On the other hand, the layer thickness experimentally observed in this regime is $\delta \gtrsim 10\rho_e$ indicating that the mechanisms supporting reconnection electric field in the experiment are fundamentally different from those in the 2D simulations. An unequivocal conclusion regarding the role of the observed fluctuations can be reached by comparing the experimentally observed thickness of reconnection layer between cases with and without fluctuations in the regime $E/E_{\mathrm{Dreicer}} \gtrsim 1$. Crucially, the minimum layer thickness in the experiment is the same *regardless of whether instabilities are present or not* (see Fig. 8). This likely indicates that fluctuations are not primarily responsible for setting the observed minimal thickness and puts into question the magnitude of the contribution of the observed fluctuations to anomalous momentum transport in the experiment.

The results presented here imply that identification of the reconnection mechanism operating in MRX weakly collisional regimes remains elusive. There currently exist no firm understanding of the mechanism that sets the thickness of the layer to be $\delta \gtrsim 10\rho_e$ in the discharges with $E > E_{\mathrm{Dreicer}}$. Over the last decade, a number of possibilities have been considered and ruled out with varying degree of confidence. Among them are the influence of infrequent Coulomb collisions,[17] presence of a neutral population (e.g., Ref. 35, see also Ref. 36), and perturbations introduced by probes.[14,37] More recent suggestions include possible presence of small-scale flux ropes within the MRX reconnection layers,[37] or influence of a weak guide field (e.g., Ref. 38). Given the results presented here, a more careful analysis of all of these possibilities needs to be carried out.

V. SUMMARY AND CONCLUSIONS

In this paper, we explored the influence of current-aligned instabilities on reconnection in the parameter regimes typical of MRX. Specifically, we compared properties of electromagnetic fluctuations observed in MRX with the results of collisionless and weakly collisional 3D fully kinetic simulations. The main conclusions from this integrated study are as follows:

(1) Simulations indicate the instability of lower-hybrid origin previously identified using linear theory[19] and collisionless simulations persists in weakly collisional regimes achievable in MRX. The mode produces substantial perturbations of the magnetic field and is characterized by $k \sim (\rho_e \rho_i)^{-1/2}$. The spectral properties and localization of the magnetic fluctuations observed in MRX are consistent with the properties of this instability.
(2) The instability identified here tends to modify the average momentum balance and broaden the current layer. However, the simulations indicate that it does not reach significant amplitude under parameters typical of MRX. Consequently, it should produce relatively small contributions to the momentum balance and moderate increase in the thickness of reconnection layer compared to the cases where the instability is absent.

(3) In order to corroborate these predictions, we analyzed how the thickness of experimentally observed reconnection layers δ changes with collisionality. The basic dependence of δ on the ratio of reconnection field to the Dreicer limit E_{Drecicer} is consistent with the results of existing simulations. However, the width of the experimentally observed reconnection layers is significantly higher than predicted by simulations in the regimes $E \gtrsim E_{\mathrm{Drecicer}}$.

(4) The characteristic minimum thickness of reconnection layers observed in the experiments is about $\delta \approx (10-15)\rho_e$ regardless of whether instabilities are present or not. This likely indicates that fluctuations are not primarily responsible for capping the minimal thickness and puts into question the magnitude of the contribution of the observed fluctuations to anomalous momentum transport in the experiment.

ACKNOWLEDGMENTS

We gratefully acknowledge support the from NSF/DOE program on basic plasma physics (Award No. 1202018), the U.S. Department of Energy through the LANL/LDRD Program, and from NASA's Heliophysics Theory Program. Contributions from MRX group were partially supported by DOE Office of Sciences—Fusion Energy Science under Contract No. DE-AC02-09CH11466 and NASA Geospace Science Award NNH10AO47I. S.D. was supported by a DOE FES Fellowship and the NDSEG Fellowship Program. Some of the simulations were performed on Roadrunner supercomputer at LANL supported through the Advanced Simulation and Computing program. In addition, this research utilized computational resources of the following centers: Oak Ridge Leadership Computing Facility at the Oak Ridge National Laboratory, which is supported by the Office of Science of the U.S. Department of Energy under Contract No. DE-AC05-00OR22725; National Energy Research Scientific Computing Center, which is supported by the Office of Science of the U.S. Department of Energy under Contract No. DE-AC02-05CH11231. Additional simulations were performed using resources provided by the NASA High-End Computing (HEC) Program through the NASA Advanced Supercomputing (NAS) Division at Ames Research Center.

[1]N. A. Krall and P. C. Liewer, Phys. Rev. A **4**, 2094 (1971).
[2]R. C. Davidson, N. T. Gladd, C. S. Wu, and J. D. Huba, Phys. Fluids **20**, 301 (1977).
[3]J. D. Huba, N. T. Gladd, and K. Papadopoulos, Geophys. Res. Lett. **4**, 125, doi:10.1029/GL004i003p00125 (1977).
[4]C. Cattell, J. Wygant, F. S. Mozer, T. Okada, K. Tsuruda, S. Kokubun, and T. Yamamoto, J. Geophys. Res. **100**, 11823, doi:10.1029/94JA03146 (1995).
[5]S. D. Bale, F. S. Mozer, and T. Phan, Geophys. Res. Lett. **29**, 2180 (2002).
[6]M. Zhou, X. H. Deng, S. Y. Li, Y. Pang, A. Vaivads, H. Reme, E. Lucek, S. Fu, X. Lin, Z. G. Yuan *et al.*, J. Geophys. Res. Space. Phys. **114**, A02216 (2009).
[7]J. P. Eastwood, T. D. Phan, S. D. Bale, and A. Tjulin, Phys. Rev. Lett. **102**, 035001 (2009).
[8]F. S. Mozer, D. Sundkvist, J. P. McFadden, P. L. Pritchett, and I. Roth, J. Geophys. Res. **116**, A12224, doi:10.1029/2011JA017109 (2011).
[9]C. Norgren, A. Vaivads, Y. V. Khotyaintsev, and M. André, Phys. Rev. Lett. **109**, 055001 (2012).
[10]T. A. Carter, M. Yamada, H. Ji, R. M. Kulsrud, and F. Trintchouk, Phys. Plasmas **9**, 3272 (2002).
[11]H. T. Ji, S. Terry, M. Yamada, R. Kulsrud, A. Kuritsyn, and Y. Ren, Phys. Rev. Lett. **92**, 115001 (2004).
[12]W. Fox, M. Porkolab, J. Egedal, N. Katz, and A. Le, Phys. Plasmas **17**, 072303 (2010).
[13]M. Yamada, H. Ji, S. Hsu, T. Carter, R. Kulsrud, N. Bretz, F. Jobes, Y. Ono, and F. Perkins, Phys. Plasmas **4**, 1936 (1997); in 38th Annual Meeting of the Division-of-Plasma-Physics of the American-Physical-Society, Denver, Colorado, November 11–15, 1996.
[14]H. Ji, Y. Ren, M. Yamada, S. Dorfman, W. Daughton, and S. P. Gerhardt, Geophys. Res. Lett. **35**, L13106, doi:10.1029/2008GL034538 (2008).
[15]Y. Ren, M. Yamada, H. Ji, S. Gerhardt, and R. Kulsrud, Phys. Rev. Lett. **101**, 085003 (2008).
[16]S. Dorfman, W. Daughton, V. Roytershteyn, H. Ji, Y. Ren, and M. Yamada, Phys. Plasmas **15**, 102107 (2008).
[17]V. Roytershteyn, W. Daughton, S. Dorfman, Y. Ren, H. Ji, M. Yamada, H. Karimabadi, L. Yin, B. J. Albright, and K. J. Bowers, Phys. Plasmas **17**, 055706 (2010).
[18]J. D. Scudder, R. D. Holdaway, W. S. Daughton, H. Karimabadi, V. Roytershteyn, C. T. Russell, and J. Y. Lopez, Phys. Rev. Lett. **108**, 225005 (2012).
[19]W. Daughton, Phys. Plasmas **10**, 3103 (2003).
[20]R. Horiuchi and T. Sato, Phys. Plasmas **6**, 4565 (1999).
[21]K. Fujimoto, Phys. Plasmas **16**, 042103 (2009).
[22]K. Fujimoto, Phys. Plasmas **18**, 111206 (2011).
[23]V. Roytershteyn, W. Daughton, H. Karimabadi, and F. S. Mozer, Phys. Rev. Lett. **108**, 185001 (2012).
[24]P. L. Pritchett and F. S. Mozer, J. Geophys. Res. Space. Phys. **116**, 7 (2011).
[25]F. S. Mozer, M. Wilber, and J. F. Drake, Phys. Plasmas **18**, 102902 (2011).
[26]K. J. Bowers, B. J. Albright, B. Bergen, L. Yin, K. J. Barker, and D. J. Kerbyson, in *Proceedings of the ACM/IEEE Conference on Supercomputing, Austin 2008* (IEEE, New York, 2008), pp. 1–11.
[27]K. J. Bowers, B. J. Albright, L. Yin, B. Bergen, and T. J. T. Kwan, Phys. Plasmas **15**, 055703 (2008).
[28]W. Daughton, J. Scudder, and H. Karimabadi, Phys. Plasmas **13**, 072101 (2006).
[29]T. Takizuka and H. Abe, J. Comput. Phys. **25**, 205 (1977).
[30]D. S. Lemons, D. Winske, W. Daughton, and B. Albright, J. Comput. Phys. **228**, 1391 (2009).
[31]W. Daughton, V. Roytershteyn, B. J. Albright, H. Karimabadi, L. Yin, and K. J. Bowers, Phys. Plasmas **16**, 072117 (2009).
[32]W. Daughton, V. Roytershteyn, B. J. Albright, H. Karimabadi, L. Yin, and K. J. Bowers, Phys. Rev. Lett. **103**, 065004 (2009).
[33]S. Hsu, T. A. Carter, G. Fiksel, H. Ji, R. M. Kulsrud, and M. Yamada, Phys. Plasmas **8**, 1916 (2001).
[34]T. Carter, H. Ji, F. Trintchouk, M. Yamada, and R. Kulsrud, "Measurement of lower-hybrid drift turbulence in a reconnecting current sheet", Phys. Rev. Lett. **88**, 015001 (2001).
[35]F. Trintchouk, M. Yamada, H. Ji, R. M. Kulsrud, and T. A. Carter, Phys. Plasmas **10**, 319 (2003).
[36]E. G. Zweibel, E. Lawrence, J. Yoo, H. Ji, M. Yamada, and L. M. Malyshkin, Phys. Plasmas **18**, 111211 (2011).
[37]S. Dorfman, Ph.D. dissertation, Princeton University, 2012.
[38]M. V. Goldman, G. Lapenta, D. L. Newman, S. Markidis, and H. Che, Phys. Rev. Lett. **107**, 135001 (2011).